





Surfactant behavior and limited incorporation of indium during *in situ* doping of GeSn grown by molecular beam epitaxy

Andrea Giunto , Louise E. Webb , Thomas Hagger , and Anna Fontcuberta i Morral 

Laboratory of Semiconductor Materials, Institute of Materials,
École Polytechnique Fédérale de Lausanne, 1015 Lausanne, Switzerland

 (Received 29 September 2022; revised 17 March 2023; accepted 2 June 2023; published 17 July 2023)

GeSn is a promising group-IV semiconductor material for on-chip Si photonics devices and high-mobility transistors. These devices require the use of doped GeSn regions, achieved preferably *in situ* during epitaxy. From the electronic valence point of view, *p*-type dopants of group-IV materials include B, Al, Ga, and In. The latter element has never been investigated as *p*-type dopant in GeSn. In this work, we explore *in situ* In *p*-type doping of GeSn grown by molecular beam epitaxy. We demonstrate that In acts as a surfactant during epitaxial growth of GeSn:In, accumulating on surface and inducing Sn segregation in the form of mobile Sn-In liquid droplets, strongly affecting the local composition of the material. In nondefective GeSn, we measure a maximal In incorporation of $2.8 \times 10^{18} \text{ cm}^{-3}$, which is two orders of magnitude lower than the values reported in the literature for *in situ p*-type doping of GeSn. We further show that In induces the nucleation of defects at low growth temperatures, hindering out-of-equilibrium growth processes for maximization of dopant incorporation. This work provides insights on the limitations associated with *in situ* In doping of GeSn and discourages its utilization in GeSn-based optoelectronic devices.

DOI: [10.1103/PhysRevMaterials.7.074605](https://doi.org/10.1103/PhysRevMaterials.7.074605)

I. INTRODUCTION

In the past decade, GeSn has been extensively studied as a novel semiconductor material for optoelectronic devices directly integrated on Si platforms [1–5]. Epitaxial integration of $\text{Ge}_{1-x}\text{Sn}_x$ on Si is enabled by their similar-sized diamond-like crystal structure, with a lattice mismatch equal to 4.2% for $x = 0$. The increase in lattice mismatch with increasing x poses however challenges in the management and limitation of detrimental relaxation defects in the material. In addition, $\text{Ge}_{1-x}\text{Sn}_x$ is a metastable material for $x > 0.01$ and thus its synthesis requires low-temperature, out-of-equilibrium processes where Ge-Sn phase separation is kinetically hindered. Above the material critical stability temperature, which is inversely related to the Sn fraction in the alloy, Sn segregates out of GeSn lattice, clustering in the bulk and forming mobile Sn droplets on the film surface [6–9].

In spite of these challenges, the promising optoelectronic properties of GeSn drove research efforts in the development of this material. $\text{Ge}_{1-x}\text{Sn}_x$ possesses a direct band gap in the near- and short-wave infrared wavelengths for approximately $x > 8.5\%$ at. [10,11], motivating the fabrication of GeSn light emitting devices (LEDs) [12–14], lasers [11,15,16], and photodiodes [17–19] for on-chip Si photonics [1]. Furthermore, GeSn theoretical carrier mobility values larger than Si and Ge [20,21] pushed for the realization of GeSn high-mobility field-effect transistors (FET) [22–24]. These (opto)electronic devices necessitate *p*-type and/or *n*-type doped regions, obtained through incorporation in the GeSn lattice of elements from respectively columns III (B, Al, Ga, In) and V (P, As, Sb)

of the Periodic Table. Incorporation of doping elements can be achieved through ion implantation or *in situ* during growth of GeSn, whereas high-temperature diffusion processes to dope GeSn from the gas phase cannot be employed due to the material metastability. In general, to avoid lattice damage and amorphization from implantation, it is desirable to dope GeSn *in situ* during growth, though this method requires thorough investigation of growth parameters to accurately calibrate dopant concentrations in the film. In addition, one needs to verify that the introduced dopants are not detrimental for the film growth process.

Several studies have demonstrated *in situ* doping of epitaxial GeSn by chemical vapor deposition (CVD) [25–29] and molecular beam epitaxy (MBE) [30–34]. While both *n*-type and *p*-type doping have been realized, the focus of this paper is exclusively on *p*-type doping. Previous works on *in situ p*-type doping of GeSn revolved around only two group-III dopant elements, namely B and Ga. The highest active *p*-type dopant concentration of $3.2 \times 10^{20} \text{ cm}^{-3}$ was reported both by Vohra *et al.* [25] for GeSn:B grown by CVD and by Wang *et al.* [32] for GeSn:Ga grown by MBE. Though this maximal active concentration is in principle sufficient for most applications, it is desirable to explore different possibilities of *in situ p*-type doping, namely using In and Al as dopant elements. Their demonstration would increase the number of options available to fabricate (opto)electronic devices with different combinations of material systems (e.g., III-V/IV heterojunction tunnel FETs [35]).

Furthermore, the addition of group-III elements to epitaxy of GeSn requires special attention, in that it may alter the growth dynamics with respect to the pure GeSn system. Elements from groups III and V are known to act as surfactants during growth of group-IV Ge and Si films [36–38].

*anna.fontcuberta-morral@epfl.ch

By analogy, we could expect similar behavior for growth of GeSn, being itself from group IV. Surfactant elements tend to remain on the surface during epitaxial growth: when buried by a surface monolayer, they exchange their position with the surface adatom; with this exchange process being faster than the characteristic time for monolayer growth, surfactants escape the subsurface layer before getting buried underneath newly grown monolayers [39]. This signifies that surfactant doping elements tend not to incorporate in the growing film and thus cannot dope it in significant concentrations. Nevertheless, despite the fact that the surfactant effect can strongly alter dopant incorporation, it is rarely discussed in the literature whether group III dopants act as surfactants during GeSn growth. To the extent of our knowledge, only Shimura *et al.* [30] took this phenomenon into consideration in their study on GeSn:Ga grown by MBE: while Ga acts as a surfactant in pure Ge epitaxial growth, they demonstrated the loss of its surfactant properties when Sn was added in the growth of GeSn. Hence they could show that Ga is an optimal element for *in situ* *p*-type doping of GeSn.

To expand the range of *p*-type doping options for the GeSn system, in this study we explore *in situ* indium doping of GeSn grown by MBE. Indium is known to possess a low solubility in pure Ge ($\sim 4 \times 10^{18} \text{ cm}^{-3}$) compared to the other group-III dopant elements, e.g., Ga, with solubility of $4.9 \times 10^{20} \text{ cm}^{-3}$ [40]. Expecting a similar behavior in GeSn, In doping of the alloy would be in principle discouraged. However, in low-temperature out-of-equilibrium epitaxial growth, elements can be incorporated in the films above their solubility limit, as is the case for Sn in Ge. It is thus worth investigating the out-of-equilibrium incorporation of indium in GeSn films. In this work, we show that the In dopant element influences the growth dynamics of the GeSn alloy. We prove that the presence of In during growth enhances defect nucleation and facilitates the segregation of Sn, inducing the formation of In-Sn liquid droplets if the growth conditions are not properly selected. With secondary-ion mass spectroscopy (SIMS) characterization, we demonstrate that In acts as a surfactant in this growth system, accumulating on the GeSn surface as the film grows. Finally, we elucidate the possible thermodynamic contributions causing enhanced surface Sn segregation in the presence of In and we discuss the limitations of In doping of GeSn alloys.

II. EXPERIMENTAL METHODS

Intrinsic Ge(001) substrates were exposed to a O_2 plasma to remove organic contaminants from the surface and were dipped in HF 1% for 90 s to remove the Ge native oxide. Substrates were then rinsed in DI water and dried with a N_2 blowing gun. After chemical cleaning, they were introduced in a Veeco GENxplor MBE growth system and degassed in the load lock at 150 °C for 30 min. The substrates underwent a further degassing step in a preparation module at 600 °C before being introduced in the growth chamber. Here, they underwent a second deoxidation step at 750 °C for 15 min. Epitaxial, monocrystalline GeSn:In films were grown by evaporating Ge, Sn, and In from individual Knudsen cells. The base pressure of the growth chamber at the start of the growth was of the order of 1×10^{-10} Torr. Substrate nominal

TABLE I. MBE deposition parameters of $\text{Ge}_{1-x}\text{Sn}_x$:In films studied in this work. All films are monocrystalline, pseudomorphic on Ge(001). The Ge flux was fixed at 1000 nTorr for all samples. Fluxes are reported in nTorr, as per measurement from the MBE beam flux monitor. Minor effective flux variations from growth to growth resulted in slight variability in GeSn thickness and alloy compositions despite constant substrate temperature (T) and Sn/Ge flux ratios, e.g., samples A, B, and C.

ID	Sub. T (°C)	Sn flux (nTorr)	In flux (nTorr)	Gr. time (min)	Thick. (nm)	x_{Sn} (% at.)	In-plane str. (%)
A	205	50	0.5	30	547	1.8	-0.26
B	205	50	1	30	542	2.0	-0.30
C	205	50	3	30	552	1.7	-0.26
D	205	100	1	30	565	3.8	-0.56
E	205	150	0.5	30	592	5.7	-0.82
F	205	150	1	30	590	5.9	-0.85
G	205	150	3	30	571	^a	^a
H	195	150	1	30	580	5.3	-0.78
I	185	150	1	30	583	5.4	-0.80
J	205	150	1	10	183	5.7	-0.85
K	205	150	1	20	404	5.4	-0.80

^aSn is fully segregated out of the film. See SEM image in Fig. 1 and XRD RSM in Fig. SM2 [41].

temperatures were calibrated with an infrared thermal camera and ranged from 185 °C to 205 °C, with uncertainty of ± 20 °C. Growth parameters for the different samples grown in this work are reported in Table I, with additional details in Table SM1 in the Supplemental Material [41]. Growths of samples E, F, and I were repeated to confirm the reproducibility of the observed physical phenomena.

Film morphology and thickness were characterized with a Zeiss Merlin scanning electron microscope (SEM). Epitaxial relation of GeSn:In films with the Ge substrates was demonstrated by x-ray diffraction reciprocal space mapping (XRD RSM) with an *X-ray Bruker D8 Discover*. The measured RSM, reported in Fig. SM2 [41], were used to calculate film composition and strain. Indium incorporation, being lower than 0.01% at., does not appreciably influence the macroscopic lattice parameter of the GeSn alloy measured with XRD and we thus used Vegard's law to calculate GeSn composition without any bowing correction [42]. In a FEI Talos system, monocrystallinity was confirmed by transmission electron microscopy (TEM) and local composition was probed with scanning TEM energy-dispersive x-ray spectroscopy (STEM EDX). Both characterizations were performed on cross-sectional lamellae cut out of the film with a Zeiss NVision focused ion beam (FIB).

The In concentration of few samples was measured via SIMS depth profiling, performed by EAG laboratories. To characterize the In concentration at the GeSn:In films surface, prior to SIMS analysis these samples were covered with 100 nm of Ge deposited by electron-beam evaporation in a separate vacuum system. No heating was applied to the sample during Ge deposition. The In concentration was calibrated using Ge:In standards as GeSn:In standards were unavailable, leading to a 15% uncertainty on the reported In concentration values. SIMS profiling was also used to verify that the

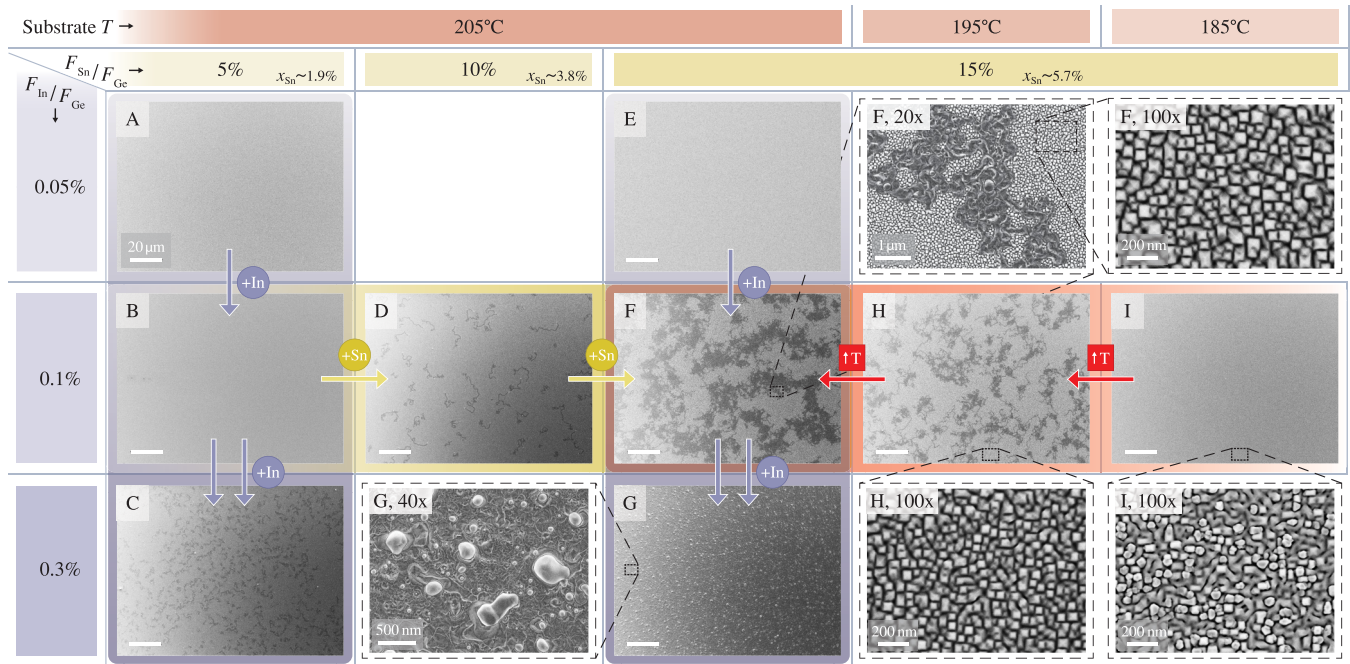


FIG. 1. SEM top-view images of monocrystalline GeSn:In films grown on Ge(001) substrates by MBE. Scale bars are 20 μm , unless differently specified. The first row shows the substrate growth temperature (T), while the first column and the second row show respectively the In/Ge and Sn/Ge flux ratios (respectively $F_{\text{In}}/F_{\text{Ge}}$, $F_{\text{Sn}}/F_{\text{Ge}}$) used during deposition of the different films. In the second header row we report also the approximate Sn atomic fraction (x_{Sn}) corresponding to the $F_{\text{Sn}}/F_{\text{Ge}}$ ratio. In the inset of each figure is the sample ID, as per Table I. A 20 \times magnification on sample F shows the formation of liquid segregation droplets and the characteristic trails they leave behind. These trails confer a darker SEM contrast that allows one to evaluate the extent of segregation simply from top-view SEM imaging. Color schemes and arrows show that by increasing the substrate temperature, In flux, and/or Sn fraction, segregation increases, and eventually covers the entire sample surface, as in the case of sample G. Images magnified by 100 \times of samples F, H, I show the typical surface morphology of GeSn:In films at different substrate T .

Sn composition across the film thickness was uniform (see Fig. SM4 [41]), as expected from GeSn MBE-grown films with Sn concentrations below 10% at. [43].

III. RESULTS

Monocrystalline GeSn:In epitaxial films with uniform Sn composition were grown on Ge(001) substrates by MBE to investigate *in situ* p -type doping of GeSn by In. Growth parameters and film characteristics of these samples are reported in Table I. Except for sample G, where Sn is almost fully segregated out of the film, all GeSn:In films are pseudomorphic, fully strained, with the absolute value of in-plane compressive strain being determined by the GeSn alloy composition. Values of GeSn composition and in-plane strain for partially segregated samples C, D, F, and H refer to the nonsegregated regions of these samples.

A. Cosegregation of In and Sn

In Fig. 1, we report top-view SEM images of a combination of different epitaxial GeSn:In films on Ge(001), grown varying substrate temperature, GeSn alloy composition, and In dopant flux. The sample label at the top-left of each SEM image refers to the growth parameters reported in Table I. Samples C, D, F, and H show regions of dark SEM contrast in a lighter background, while all other samples, with the

exception of sample G, at low magnification present a surface with homogeneous light SEM contrast. The 20 \times magnified SEM image of sample F reveals the origin of dark SEM contrast: liquid droplets have formed and moved around during growth, leaving behind a trail that appears darker at SEM. This phenomenon resembles closely that of Sn segregation in pure GeSn epitaxy, modeled in Refs. [7,9]: Sn segregates out of the Ge matrix and forms liquid droplets on the surface. These segregation droplets move around during growth dissolving the GeSn film at their front and depositing behind a trail of almost pure Ge.

To understand the origin of droplet formation, we performed TEM characterization on sample F, presented in Fig. 2. The top-view SEM image in Fig. 2(a) illustrates the surface morphology of sample F, more neatly visible in Fig. 1 (F, 20 \times and 100 \times) and in Fig. SM7 [41]. A dashed, black rectangle in Fig. 2(a) indicates the region probed by TEM in Fig. 2(b), which contains a liquid droplet, part of the droplet trail, and portions of pristine, nonsegregated GeSn:In film. TEM bright-field (BF) imaging in Fig. 2(b) shows defects underneath the segregation regions (i.e., droplet and its trail), which seem to indicate a boundary with pristine GeSn:In film, confirmed to be monocrystalline in the inset TEM diffractogram. Segregation thus appears to occur only in the surface region, suggesting droplet nucleation takes place at a late stage of growth. In addition, we observe that the segregation droplet does not dissolve the entire film underneath, which remains

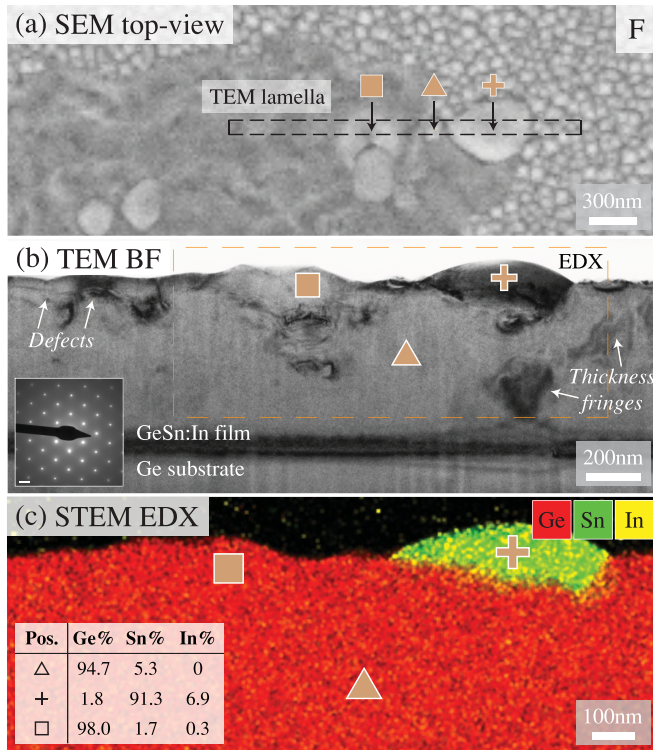


FIG. 2. (a) Top-view SEM image of segregation droplets and trails on sample F. (b) TEM bright field image of the region framed within a dashed, black rectangle in (a). The diffraction pattern in the inset, with scale bar of 2 nm^{-1} , demonstrates single crystallinity of the GeSn:In film. Orange symbols indicate the positions probed by STEM EDX in (c), with the corresponding measured atomic compositions reported in the table inset. EDX shows that the segregation droplet (+) is mainly composed of Sn and In. The droplet trail (□) is instead almost pure Ge, as expected from previous works. Full measurement details are reported in Fig. SM8 [41].

unaffected. The TEM contrast visible underneath the droplet is in fact only due to thickness fringes (see also Fig. SM8 [41]). This is contrary to what was reported in Refs. [7,9], where the droplet entirely dissolved the GeSn film on its path. This apparent disagreement can, however, be explained by the large difference in thickness between the studied films: while in Refs. [7,9] the GeSn film had a thickness of $\sim 50 \text{ nm}$, sample F is 590 nm thick.

Orange symbols in Fig. 2 indicate the positions probed by STEM EDX in Fig. 2(c), with the relative measured atomic compositions reported in the table inset. Single elemental maps and additional measurement details are reported in Fig. SM8 [41]. As a reference, we consider first the GeSn composition in the pristine region of the monocrystalline GeSn:In film (Δ). Here, STEM EDX detects a Sn concentration of $(5.3 \pm 0.6)\%$ at., close within error to the real GeSn composition measured by XRD. No In is detected in Δ , indicating that its concentration in the film is below the EDX detection limit. On the other hand, in correspondence with the segregation droplet (+) STEM EDX reveals major concentrations of Sn and In, respectively of $(91.3 \pm 1.0)\%$ at. and $(6.9 \pm 0.9)\%$ at. Here, Ge is only detected with a concentration of $(1.8 \pm 0.2)\%$ at., near its solubility limit in pure

Sn at the growth temperature of this sample [44]. The droplet trail (\square), as expected from previous works [7,9], is composed of almost pure Ge, with minimal fractions of In and Sn trapped during Ge precipitation from the droplet. These observations suggest that droplet formation is the result of Sn-In cosegregation, as later elaborated in Sec. IV.

Having verified that segregation droplets are composed of Sn-In, we can now shift our attention back to Fig. 1. Here, the arrows show that substrate temperature (red), In flux (purple), and Sn flux (yellow) are parameters that can initiate or increment the extent of Sn-In segregation. In particular, we can observe the following effects of the fluxes: at a nominal substrate temperature of $205 \text{ }^\circ\text{C}$, samples with a In/Ge flux ratio of 0.05% (samples A, E) show no sign of segregation. On the other hand, by increasing the In/Ge flux ratio to 0.1% , we observe segregation for $F_{\text{Sn}}/F_{\text{Ge}} = 10\%$ (sample D, $x_{\text{Sn}} = 3.8\%$ at.) and $F_{\text{Sn}}/F_{\text{Ge}} = 15\%$ (sample F, $x_{\text{Sn}} = 5.9\%$ at.). It is remarkable that a small $F_{\text{In}}/F_{\text{Ge}}$ increase of 0.05% causes Sn-In segregation, considering that even an increase of 10% in $F_{\text{Sn}}/F_{\text{Ge}}$ from sample A to E does not induce it. Therefore, In seems to have a considerably stronger effect on segregation than Sn and we will discuss this phenomenon later in Sec. IV A. A further increase of $F_{\text{In}}/F_{\text{Ge}}$ to 0.3% induces partial segregation in $\text{Ge}_{0.981}\text{Sn}_{0.019}$ (sample C) and full segregation in $\text{Ge}_{0.943}\text{Sn}_{0.057}$ (sample G), clearly visible in the magnified SEM image (G, $40\times$).

Besides the In flux, we can observe that also the Sn flux has an effect on the extent of segregation: at constant substrate temperature, increasing $F_{\text{Sn}}/F_{\text{Ge}}$ from 10% ($x_{\text{Sn}} \sim 3.8\%$) to 15% ($x_{\text{Sn}} \sim 5.7\%$) in the presence of $F_{\text{In}}/F_{\text{Ge}} = 0.1\%$ (respectively samples D and F) considerably increases the fraction of surface covered by segregated regions. Finally, increasing the substrate temperature (from sample I grown at $185 \text{ }^\circ\text{C}$ to H at $195 \text{ }^\circ\text{C}$ to F at $205 \text{ }^\circ\text{C}$) also induces segregation. While the increase of Sn flux and substrate temperature are expected from previous studies to favor segregation in GeSn alloys [6–9], the impact of In on segregation phenomena in GeSn remains to be elucidated.

B. Defective growth at low temperature

As expected, decreasing the substrate temperature from sample F can reduce (sample H) and prevent (sample I) Sn-In cosegregation. This, however, comes at the cost of film crystal quality. In Fig. 1, the $100\times$ zoomed SEM top-view images of nonsegregated regions show regularly faceted surface features for substrate temperatures of $195 \text{ }^\circ\text{C}$ (H, $100\times$) and $205 \text{ }^\circ\text{C}$ (F, $100\times$) corresponding to monocrystalline, pseudomorphic GeSn:In. On the other hand, in sample I, grown at a lower T of $185 \text{ }^\circ\text{C}$, the surface morphology is irregular and epitaxy seems broken at the brighter grains. Indeed, cross-sectional TEM BF of this sample in Fig. 3(a) shows that pseudomorphic epitaxial growth locally breaks down after the film reaches a thickness of about 400 nm , forming defective regions that extend to the film surface. A magnified TEM image of one of these defective regions is reported in Fig. 3(b). Here, defect nucleation during growth yields surface asperities (red arrows) that are taller and of higher aspect ratio compared to the rest of the surface (green arrows), conferring them the bright contrast observed at SEM.

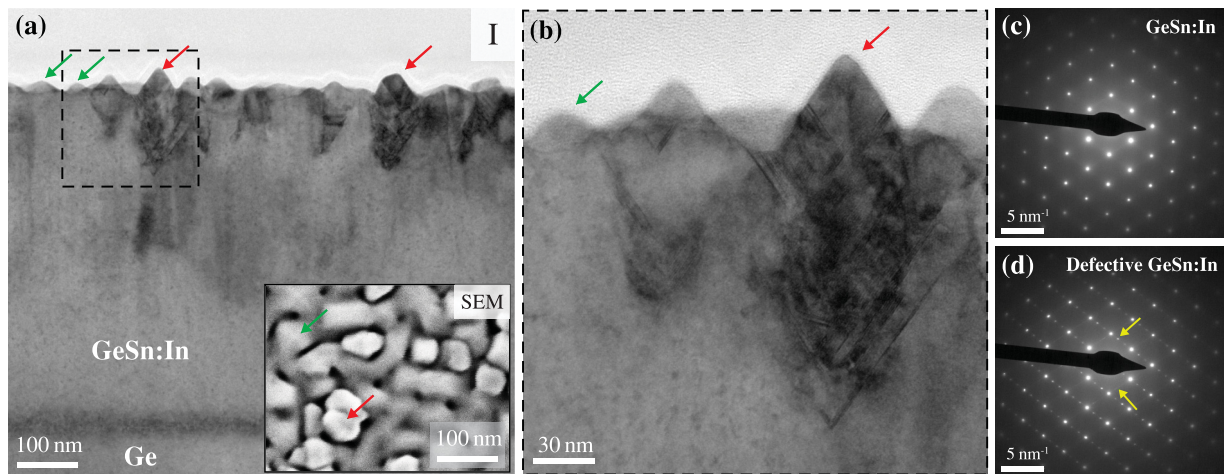


FIG. 3. (a) Cross-sectional TEM bright-field image of sample I, grown with a nominal substrate temperature of 185 °C. The inset shows a top-view SEM image of the sample surface. Red and green arrows mark respectively defective and nondefective regions. (b) Zoomed TEM bright-field image of the region enclosed within the black, dashed square in (a), showing clearly the presence of defects at these regions. (c) TEM diffraction pattern of nondefective GeSn:In showing only diffraction spots corresponding to $\langle 110 \rangle$ zone axis. (d) TEM diffraction pattern of defective region in (b), showing additional diffraction spots and streaks (yellow arrows) due to the presence of stacking faults. Additional details on these measurements are in Fig. SM9 [41].

By means of TEM diffraction, we identified the type of defects forming at 185 °C in sample I. Figure 3(c) shows a reference TEM diffraction pattern of the nondefective region of the GeSn:In film. Here, only diffraction spots corresponding to monocrystalline GeSn:In aligned along the $\langle 110 \rangle$ zone axis are visible. The TEM diffraction pattern in Fig. 3(d) of the defective region in Fig. 3(b) shows two additional distinctive features indicated by yellow arrows: (1) striking of diffraction spots and (2) additional diffraction spots positioned between the spots belonging to the $\langle 110 \rangle$ zone axis. While the former originates from the presence of stacking faults, the latter is a more peculiar feature, appearing in our case due to periodically arranged stacking faults. A more detailed analysis of these features is out of the scope of this manuscript and is thus briefly reported in Fig. SM9 [41]. In the latter figure, we also show the presence of polycrystallinity in sample I in correspondence with some defects, indicating local breakdown of epitaxy. This behavior has been previously observed in MBE growth of GeSn at $T < 155$ °C and was attributed to kinetic roughening effects [45,46]. Kinetic roughening describes a system where adatom mobility is strongly reduced by the low growth temperatures, leading to significant surface roughening that induces defect nucleation. This results in a switch from monocrystalline to polycrystalline growth and eventually to amorphous deposition [47].

Lastly, we stress that the growth of sample I has been repeated to confirm the behavior reported in Fig. 3 and that the observed defects are not present in pure GeSn grown at 185 °C (see Fig. SM3 [41]). These results therefore suggest that at low growth temperature the presence of In has an additional detrimental effect during epitaxy of GeSn alloys, related to reduced Sn and Ge adatom diffusion [46] and/or accumulation of surfactant-induced defects on the surface [48].

C. Surfactant effect of In

To understand whether In acts as a surfactant during growth, aiding surface segregation, we performed SIMS depth

profiling of the In concentration in three GeSn:In films. The results are shown in Fig. 4. We selected samples without surface segregation, namely B (purple), E (orange), and I (green), in order to avoid In concentration artifacts due to Sn-In segregation droplets. Samples B and E were grown at 205 °C using different Sn and In fluxes, while sample I was grown at 185 °C. All SIMS profiles show that the In concentration increases along the film thickness, denoting an increment in In incorporation rate as the film grows. This indicates that In is acting as a surfactant, accumulating on surface during growth and driving a proportional increase in In incorporation [49] across the entire range of temperatures considered in this study. The In surfactant behavior is confirmed by the peaks of two-order-of-magnitude higher In concentration detected at the films surface (indicated by arrows in Fig. 4), pointing at an accumulation of the dopant on surface. Furthermore, in sample I we note a strong increase in In concentration already around 400 nm, corresponding to the onset of defect nucleation observed in Fig. 3. This suggests defects can more easily accommodate In dopant incorporation.

D. Measured In concentrations in GeSn:In

By comparing the In atomic concentrations in the different samples in Fig. 4, we observe that the In incorporation in the nondefective region of sample I (up to 400 nm) is considerably lower despite its In flux being equal to sample B and double of sample E. This suggests the In incorporation rate decreases when lowering the growth temperature, possibly due to a reduction of In solubility in Ge [40]. Furthermore, considering the two samples grown at 205 °C, more In has been incorporated in sample B as a result of the higher In flux used during deposition. For the same reason, sample B exhibits a higher In concentration peak on surface, though we should consider that the In surface peak of sample E is broadened by its higher film surface roughness (see details in Fig. SM1 [41]). Integration of the In surface signal yields

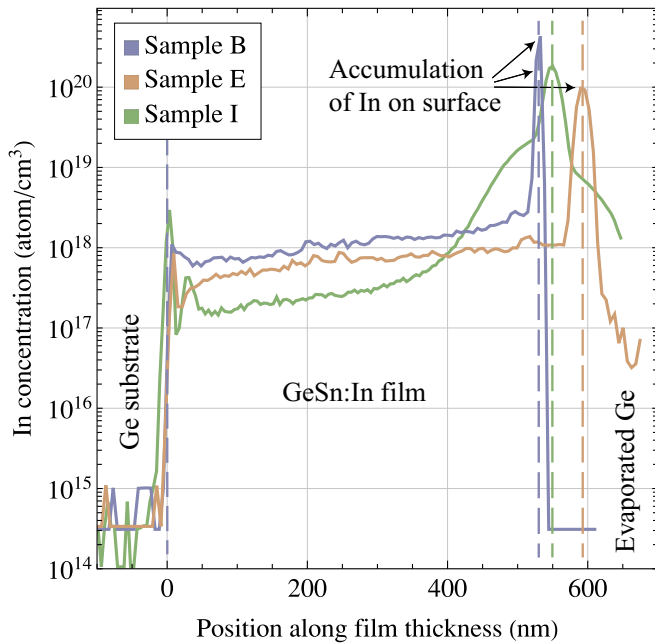


FIG. 4. SIMS depth profiling of In concentration in samples B (purple), E (orange), and I (green). Samples B and E were grown at 205 °C with different In and Sn fluxes, while sample I was grown at 185 °C. The three samples were covered by a 100-nm-thick thin film of Ge deposited by evaporation prior to SIMS characterization. SIMS shows that In incorporation increases along the film thickness at all growth temperatures, suggesting that the dopant is acting as a surfactant, accumulating on surface during growth. This is confirmed by the two-order-of-magnitude increase in In concentration on the films surface (indicated by black arrows), which shows clear accumulation of the dopant element on the surface. Indium concentration is higher in sample B with respect to sample E as a result of the higher In flux used during growth, while In incorporation seems to be reduced by the lower growth temperature in sample I. In the latter, the sharp increase of In concentration after 400 nm corresponds to the onset of defect nucleation, shown in Fig. 3, indicating a higher In incorporation rate in defects.

an atomic density of $4.0 \times 10^{14} \text{ cm}^{-2}$ and $2.0 \times 10^{14} \text{ cm}^{-2}$, respectively for sample B and E, corresponding exactly to the ratio between their In fluxes during growth.

From the SIMS depth profiling in Fig. 4 we can also extract the maximal In incorporation obtained in the nondefective GeSn:In films. As a consequence of the In surfactant behavior, the In incorporation rate increases during growth, resulting in a difference in In concentration across the film thickness of almost an order of magnitude. For both samples B and E the maximal In concentration is thus found right below the GeSn:In film surface, corresponding respectively to $2.8 \times 10^{18} \text{ cm}^{-3}$ and $1.4 \times 10^{18} \text{ cm}^{-3}$. The ratio of maximal In concentrations in the two samples matches the ratio of In fluxes used during their growths, suggesting a direct proportionality between the In flux and the In incorporation rate despite the surfactant behavior of the dopant element. It is interesting to notice that both concentrations are lower than the solid solubility of In in pure Ge, reported to be $\sim 4 \times 10^{18} \text{ cm}^{-3}$ [40]. In addition, Hall measurements of sample B, reported in Fig. SM6 [41], determined an electrically active carrier

concentration of $2.9 \times 10^{17} \text{ cm}^{-3}$ at 300 K, yielding a low activation of 24.2% with respect to the average film In concentration of $1.2 \times 10^{18} \text{ cm}^{-3}$. This may be due to In dopant clustering, known to occur in Ge [50,51], or due to incomplete dopant activation. If the latter is the case, postgrowth thermal annealing may be beneficial in increasing dopant activation, though the process would be limited by the metastability of the system and is thus preferably avoided in *in situ* doping [25,32].

IV. DISCUSSION

A. Origins of Sn-In cosegregating behavior

The results of this study indicate a tendency for Sn and In to cosegregate, forming liquid droplets on surface. During growth, these droplets move around on surface, dissolving a portion of the GeSn:In film at their front and depositing behind a trail of almost pure Ge, as elucidated in Refs. [7,9] for the pure GeSn alloy. In this section, we provide an explanation for the observed enhancement of segregation induced by In doping.

Contrary to what is observed by Shimura *et al.* in Ref. [30] for Ga, we found that In does not lose its surfactant properties in the presence of Sn at the temperatures considered in this study. Therefore, In tends to stay on surface and accumulate during growth as a result of an imbalance between incoming atomic flux and incorporation rate in the film. Intuitively, as the film grows, and the In surface concentration increases, we can expect this increase in In to be determinant in initiating segregation in the form of liquid droplets. To demonstrate it, we grew GeSn:In films with the same deposition parameters as sample F, interrupting the growth to observe the evolution of surface segregation at different film thicknesses. The SEM top-view images of samples J, K, and F, respectively grown for 10 min, 20 min, and 30 min, are shown in Fig. 5. While no segregation occurs with 10 min (183 nm) of growth, surface segregation is initiated after 20 min (404 nm) and after 30 min (590 nm) approximately half of the surface is covered by Sn-In droplets and their trails. If there was no increase in In surface concentration during growth, conditions would be stationary and thus the film thickness would not affect the extent of surface segregation. Hence these results clearly point at In surface accumulation being a driver for Sn-In segregation.

Nevertheless, the In surfactant behavior does not offer a full picture of the segregation process. At this point, it is still not clear why Sn and In cosegregate. This matter is easily resolved by looking at the InSn phase diagram [52], which predicts that at the growth temperatures used in this work Sn and In are liquid and completely miscible for alloy compositions up to 80% at. of Sn. Sn and In can thus aggregate in a single liquid phase, though some excess Sn may precipitate during the process. Secondly, the peak value of In concentration reached on the surface of sample B measured by SIMS in Fig. 4 is $5.8 \times 10^{20} \text{ at./cm}^3$ (see Fig. SM5 [41] for details on the fitting of the SIMS depth profile), which is approximately 1.2% at. of the cubic Ge atomic density of $4.41 \times 10^{22} \text{ at./cm}^3$. Sample B, with 2% at. Sn, is not segregated. However, with the same In flux, by increasing the Sn fraction to 3.8% at. (sample D) segregation occurs (see note [53] in this regard). Summing the Sn and In fractions in

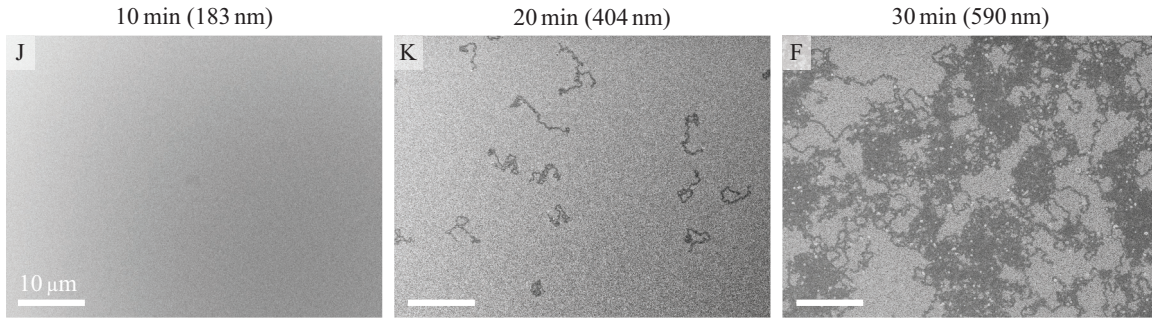


FIG. 5. SEM top-view imaging of the surface of three GeSn:In films (samples J, K, and F) grown with the same deposition parameters for different times. Surface segregation is absent after 10 min (183 nm), while after 20 min (404 nm), few Sn-In droplets with single trails can be observed. The accumulation of In surfactant on surface during growth induces more extended segregation after 30 min (590 nm) of growth.

sample D we obtain 5% at., which is well below the fraction of Sn necessary to cause segregation in intrinsic GeSn at this growth temperature (e.g., sample E, with 5.7% at. Sn, is not segregated, despite being doped with a small concentration of In). Simply put, while 5% at. Sn does not cause segregation at a nominal substrate temperature of 205 °C, 3.8% at. Sn plus 1.2% at. In do. This indicates that the increase in segregation in the presence of In is not due to a mere increase in total concentration of segregating atoms. It is rather the nature of the In+Sn system that is increasing the occurrence of surface segregation when replacing 1.2% at. Sn with 1.2% at. In (see note [54]).

To explain the influence of In, we turn to classical theory of nucleation and growth of thin films [55,56]. Droplet surface segregation can be described as the 3D nucleation of a liquid phase on the film surface. The nucleation rate (J) is then expressed with the scaling law (using the notation from Ref. [56])

$$J \propto Dn_1n_i, \quad (1)$$

where n_1 is the surface concentration of single adatoms, D is their diffusion coefficient, and n_i is the concentration of critically sized clusters. We expand the latter using

$$n_i \propto \exp[-\Delta G_i/(k_B T)], \quad (2)$$

where k_B is the Boltzmann constant, T is the substrate temperature, and ΔG_i is the Gibbs free energy of a cluster at its critical size, which can be approximated by

$$\Delta G_i \propto X^3/\Delta\mu^2, \quad (3)$$

with X being the liquid surface tension and $\Delta\mu$ the supersaturation of the liquid phase. Substituting Eqs. (2) and (3) in Eq. (1) we obtain

$$J \propto Dn_1 \exp[-X^3/(\Delta\mu^2 k_B T)]. \quad (4)$$

With Eq. (4) in mind, we can compare a system with 5% at. Sn on surface to a system with 3.8% at. Sn plus 1.2% at. In at equal temperature. We know the former system does not segregate, while the latter does. The total adatom concentration n_1 would be the same for both systems and is therefore not playing a role in the observed difference in segregation. On the other hand, the diffusion coefficient D is different for the two atomic species. In literature, we find diffusion energy barriers for In and Sn adatoms on the Si(100) surface, respectively equal to 0.27 eV [57] and 1.2 eV [58]. Due to the similarity

of group-IV materials, we can expect analogous behavior on the surface of a Ge(100) substrate and GeSn(100) film. The considerably smaller diffusion barrier for In signifies In adatoms can diffuse faster than Sn adatoms. Faster diffusion increases the adatom diffusion length and thus its likelihood of encountering and sticking to an atomic cluster. This ultimately results in greater probability of droplet nucleation.

A further element that may enhance segregation in the presence of In is the liquid surface tension X . Dadashev *et al.* report in Ref. [59] that the surface tension of the SnIn liquid is smaller by 1–2% (depending on the In atomic fraction) compared to pure Sn liquid, lowering the Gibbs free energy of critical clusters [ΔG_i , Eq. (3)]. In Ref. [59], the study included a range of temperatures between 250 °C and 450 °C, reasonably close to the growth temperatures used in this work to expect an analogous behavior of X_{SnIn} . Lastly, also the supersaturation term, inversely proportional to the equilibrium vapor pressure of the species [$\Delta\mu = k_B T \ln(p/p_e)$, with p being the partial pressure of an element and p_e its equilibrium vapor pressure], predicts an increase in segregation in the presence of In: first, $p_{e,In} < p_{e,Sn}$ [60] and, second, considering the only available data in the literature, the activity coefficient (see note [61]) of In in the SnIn melt at 400 °C is well below 1 [62,63], suggesting a further decrease in $p_{e,In}$. The activity coefficient of Sn is very close to 1 for large Sn fractions in the SnIn liquid [62,63] and should thus not play a role here. Overall, the supersaturation term $\Delta\mu$ is thus likely increased in magnitude in the presence of In at our growth temperatures, driving an increase in the nucleation rate J . To summarize, at a fixed GeSn:In growth temperature, the terms D , X , and $\Delta\mu$ from Eq. (4) hint at a higher liquid droplet nucleation rate in the presence of In, explaining the increase in segregation with respect to pure GeSn epitaxy.

Concerning the dependence of Sn-In cosegregation with temperature and Sn flux observed in Fig. 1, SIMS measurements in Fig. 4 show that within the range of growth parameters used in this work In always acts as a surfactant, inducing Sn-In segregation. In addition, from Eq. (4) we can deduce the following.

(i) A lower Sn flux trivially decreases n_1 and p_{Sn} , and thus the nucleation rate J .

(ii) The Arrhenius-type dependence of nucleation rate J on the temperature T determines a decrease in J with lower T .

(iii) The same holds for D , which is also dependent on T via an Arrhenius-type law.

(iv) The surface tension X is weakly dependent on T [59], and increases with lower T , lowering J .

(v) p_e decreases with lower T and is thus the only term positively contributing to J . Experimental data in Fig. 1, however, clearly shows that cosegregation is reduced by lowering the substrate T and thus the positive contribution from p_e must be lower than the negative contribution of all other terms of Eq. (4).

Lastly, we highlight that the present analysis focused on a narrow range of growth temperatures and that it is unclear whether In would favor segregation also below this range. Still, the results from growth at 185 °C in Fig. 3 showed that the range of usable growth temperatures for GeSn:In is limited by the presence of In itself. Even if Sn-In do not cosegregate at lower temperatures, defects will break down epitaxy, preventing low-temperature monocrystalline GeSn:In growth.

B. In solubility in GeSn

From Fig. 4, the maximal In incorporation we obtained was $2.8 \times 10^{18} \text{ cm}^{-3}$ in $\text{Ge}_{0.98}\text{Sn}_{0.02}$ (sample B), which is lower than the solubility of In in pure Ge ($\sim 4 \times 10^{18} \text{ cm}^{-3}$ [40]). All other growth parameters being equal, an increase in Sn content to 3.8% at. (sample D) and 5.7% at. (sample F) leads to progressively increased Sn-In segregation. Hence we can conclude that the solubility of In in nondefective GeSn thin films is dependent on the alloy composition and decreases with increasing Sn content. The solubility of In is thus expected to be lower in GeSn compared to pure Ge.

This dependence of In incorporation on alloy composition could arise from the compressive strain present in the pseudomorphic GeSn:In films considered in this study. As reported in Table I, compressive strain increases with Sn fraction in the alloy, disfavoring the insertion of large indium atoms in the GeSn matrix. Further experiments are required to verify if In solubility is dependent on the strain state of the thin film or if it is purely dependent on the alloy composition.

C. Maximizing In incorporation in GeSn

Considering the maximal dopant incorporation measured in this work, we note that it is substantially smaller than the maximal GeSn *in situ p-type* active doping concentrations $> 10^{20} \text{ cm}^{-3}$ reported in the literature [25,32], especially considering the low electrical dopant activation of 24.2% measured in sample B. In principle, the In concentration of $\text{Ge}_{0.98}\text{Sn}_{0.02}$ in this sample could be increased by increasing the In flux, but in Fig. 1 sample C shows that, by triplicating F_{In} , the $\text{Ge}_{0.98}\text{Sn}_{0.02}$:In film segregates. This yields $8.4 \times 10^{17} \text{ cm}^{-3}$ as the upper limit of In incorporation in nondefective GeSn at 205 °C, still considerably lower than the concentrations of *p-type* dopants found in literature.

Typically, dopant incorporation could be increased by kinetically hindering Sn-In cosegregation, i.e., lowering the growth temperature. However, the growth of sample I at 185 °C showed that also this possibility is limited, as the In incorporation rate decreases at lower temperature (Fig. 4). In addition, at the same temperature, epitaxial growth of GeSn:In starts breaking down after 400 nm (Fig. 3), while this does not occur for pure GeSn. Maintaining a GeSn:In thickness lower

than 400 nm would certainly prevent the nucleation of defects at 185 °C, but a further decrease in temperature would still be limited by the kinetic roughening effect, since the critical thickness for epitaxial breakdown is known to be reduced by lowering the growth temperature [64]. Furthermore, when employing thinner GeSn:In films, one needs nonetheless to consider that the dopant incorporation will be limited by the surfactant behavior of In, which determines a difference in concentration of almost one order of magnitude across film thicknesses of less than 600 nm, as visible in Fig. 4 for samples B and E.

Overall, this study does not aim at maximizing the In doping concentrations, but rather at elucidating the limitations associated with *in situ* In doping of GeSn. Still, the phenomena we outlined show that the practical maximal In doping concentration in nondefective GeSn:In is not too far from the values measured in our work.

V. CONCLUSIONS

The results shown in this work outline some limitations for using In as a *p-type* dopant element in GeSn. We demonstrated that In induces cosegregation with Sn, causing the formation of mobile SnIn metallic droplets on the GeSn:In film surface that could be detrimental for (opto)electronic device performance. We illustrated the enhancement in segregation as the result of multiple factors. First, In acts as a surfactant for GeSn, accumulating on the surface during growth. Secondly, In adatoms diffuse faster than Sn adatoms, increasing the probability to encounter segregating clusters and bond to form stable liquid nuclei. Thirdly, the limited data present in the literature suggest that the Gibbs free energy of formation of a critical SnIn liquid nucleus is lower compared to that of pure Sn liquid.

We observed that as a result of the surfactant effect of In, its incorporation rate increases during growth, complicating accurate control of the final dopant concentration in the film. The maximum dopant incorporation we measured in nondefective films was $2.8 \times 10^{18} \text{ cm}^{-3}$ in $\text{Ge}_{0.98}\text{Sn}_{0.02}$ with a low electrical activation of 24.2% at 300 K, far from the maximal active *p-type* dopant values $> 10^{20} \text{ cm}^{-3}$ reported in the literature for GeSn. Furthermore, we showed that the solubility of In in GeSn decreases with larger Sn fractions in the alloy, limiting the applications of GeSn:In *in situ* doping to devices that do not require significant doping concentrations. Lastly, we demonstrated that lowering the growth temperature to avoid Sn-In cosegregation and push the In incorporation is not a viable strategy for this material system, as it leads to a decrease in In incorporation rate and epitaxy breakdown due to kinetic roughening effects and/or dopant-related defect accumulation.

This work provides insights on the behavior of the indium dopant element in the GeSn system and discourages its utilization in GeSn-based optoelectronic devices.

ACKNOWLEDGMENTS

The authors wish to thank N. Singh for his help in substrate preparation and J.-B. Leran for his maintenance of the MBE. This work was supported by Innosuisse, SNSF NCCR QSIT,

Max Planck Institut für Festkörperforschung, and Max Planck Graduate Center for Quantum Materials.

A.G. and A.F.i.M. conceived the experiments. A.G. did all the experiments and analysis with the exception of Hall

measurements in Fig. SM6 [41], performed by L.E.W., and atomic force microscopy measurements in Fig. SM1 [41], performed by T.H. The manuscript was written by A.G., with inputs from A.F.i.M. and L.E.W.

-
- [1] O. Moutanabbir, S. Assali, X. Gong, E. O'Reilly, C. A. Broderick, B. Marzban, J. Witzens, W. Du, S.-Q. Yu, A. Chelnokov, D. Buca, and D. Nam, Monolithic infrared silicon photonics: The rise of (Si)GeSn semiconductors, *Appl. Phys. Lett.* **118**, 110502 (2021).
- [2] Y. Miao, G. Wang, Z. Kong, B. Xu, X. Zhao, X. Luo, H. Lin, Y. Dong, B. Lu, L. Dong, J. Zhou, J. Liu, and H. H. Radamson, Review of Si-based GeSn CVD growth and optoelectronic applications, *Nanomaterials* **11**, 2556 (2021).
- [3] J. Zheng, Z. Liu, C. Xue, C. Li, Y. Zuo, B. Cheng, and Q. Wang, Recent progress in GeSn growth and GeSn-based photonic devices, *J. Semicond.* **39**, 061006 (2018).
- [4] H. Lin, Z. Luo, T. Gu, L. C. Kimerling, K. Wada, A. Agarwal, and J. Hu, Mid-infrared integrated photonics on silicon: A perspective, *Nanophotonics* **7**, 393 (2017).
- [5] S. Wirths, D. Buca, and S. Mantl, SiGeSn alloys: From growth to applications, *Prog. Cryst. Growth Charact. Mater.* **62**, 1 (2016).
- [6] S. Mukherjee, S. Assali, and O. Moutanabbir, Atomic pathways of solute segregation in the vicinity of nanoscale defects, *Nano Lett.* **21**, 9882 (2021).
- [7] H. Groiss, M. Glaser, M. Schatzl, M. Brehm, D. Gerthsen, D. Roth, P. Bauer, and F. Schäffler, Free-running Sn precipitates: An efficient phase separation mechanism for metastable Ge_{1-x}Sn_x epilayers, *Sci. Rep.* **7**, 16114 (2017).
- [8] P. Zaumseil, Y. Hou, M. A. Schubert, N. von den Driesch, D. Stange, D. Rainko, M. Virgilio, D. Buca, and G. Capellini, The thermal stability of epitaxial GeSn layers, *APL Mater.* **6**, 076108 (2018).
- [9] A. Kuchuk, P. Lytvyn, Y. Mazur, H. Stanchu, S. Kondratenko, F. de Oliveira, S. Malyuta, M. Teodoro, M. Benamara, S.-Q. Yu, and G. Salamo, Sn-guided self-grown Ge stripes banded by GeSn Nanowires: Formation mechanism and electric-field-induced switching from p- to n-type conduction, *Appl. Surf. Sci.* **604**, 154443 (2022).
- [10] J. D. Gallagher, C. L. Senaratne, J. Kouvetakis, and J. Menéndez, Compositional dependence of the bowing parameter for the direct and indirect band gaps in Ge_{1-y}Sn_y alloys, *Appl. Phys. Lett.* **105**, 142102 (2014).
- [11] S. Wirths, R. Geiger, N. von den Driesch, G. Mussler, T. Stoica, S. Mantl, Z. Ikonik, M. Luysberg, S. Chiussi, J. M. Hartmann, H. Sigg, J. Faist, D. Buca, and D. Grützmacher, Lasing in direct-bandgap GeSn alloy grown on Si, *Nat. Photon.* **9**, 88 (2015).
- [12] C. Cardoux, L. Casiez, N. Pauc, V. Calvo, N. Coudurier, P. Rodriguez, J. Richy, P. Barritault, O. Lartigue, C. Constancias, M. Frauenrath, J.-M. Hartmann, A. Chelnokov, O. Gravrand, and V. Reboud, Room temperature spectral characterization of direct band gap Ge_{0.85}Sn_{0.15} LEDs and photodiodes, in *Silicon Photonics XVII*, March, edited by G. T. Reed and A. P. Knights (SPIE, Bellingham, WA, 2022), p. 12.
- [13] B.-J. Huang, C.-Y. Chang, Y.-D. Hsieh, R. A. Soref, G. Sun, H.-H. Cheng, and G.-E. Chang, Electrically injected GeSn vertical-cavity surface emitters on silicon-on-insulator platforms, *ACS Photon.* **6**, 1931 (2019).
- [14] C. Chang, T.-w. Chang, H. Li, H. H. Cheng, R. Soref, G. Sun, and J. R. Hendrickson, Room-temperature 2- μ m GeSn P-I-N homojunction light-emitting diode for inplane coupling to group-IV waveguides, *Appl. Phys. Lett.* **111**, 141105 (2017).
- [15] Y. Kim, S. Assali, D. Burt, Y. Jung, H.-J. Joo, M. Chen, Z. Ikonik, O. Moutanabbir, and D. Nam, Improved GeSn microdisk lasers directly sitting on Si, in *Silicon Photonics XVII*, March, edited by G. T. Reed and A. P. Knights (SPIE, Bellingham, WA, 2022), p. 21.
- [16] S. Ojo, Y. Zhou, S. Acharya, N. Saunders, S. Amoah, Y.-T. Jheng, H. Tran, W. Du, G.-E. Chang, B. Li, and S.-Q. Yu, Silicon-based electrically injected GeSn lasers, in *Physics and Simulation of Optoelectronic Devices XXX*, March, edited by M. Osiański, Y. Arakawa, and B. Witzigmann (SPIE, Bellingham, WA, 2022), p. 15.
- [17] M. R. M. Atalla, S. Assali, S. Koelling, A. Attiaoui, and O. Moutanabbir, High-bandwidth extended-SWIR GeSn photodetectors on silicon achieving ultrafast broadband spectroscopic response, *ACS Photon.* **9**, 1425 (2022).
- [18] E. Talamas Simola, V. Kiyek, A. Ballabio, V. Schlykow, J. Frigerio, C. Zucchetti, A. De Iacovo, L. Colace, Y. Yamamoto, G. Capellini, D. Grützmacher, D. Buca, and G. Isella, CMOS-Compatible Bias-Tunable Dual-Band Detector Based on GeSn/Ge/Si Coupled Photodiodes, *ACS Photon.* **8**, 2166 (2021).
- [19] H. Tran, T. Pham, J. Margetis, Y. Zhou, W. Dou, P. C. Grant, J. M. Grant, S. Al-Kabi, G. Sun, R. A. Soref, J. Tolle, Y.-H. Zhang, W. Du, B. Li, M. Mortazavi, and S.-Q. Yu, Si-based GeSn photodetectors toward mid-infrared imaging applications, *ACS Photon.* **6**, 2807 (2019).
- [20] J. D. Sau and M. L. Cohen, Possibility of increased mobility in Ge-Sn alloy system, *Phys. Rev. B* **75**, 045208 (2007).
- [21] S. Mukhopadhyay, B. Mukhopadhyay, G. Sen, and P. K. Basu, Maximum theoretical electron mobility in n-type Ge_{1-x}Sn_x due to minimum doping requirement set by intrinsic carrier density, *J. Comput. Electron.* **20**, 274 (2021).
- [22] M. Liu, K. Mertens, N. von den Driesch, V. Schlykow, T. Grap, F. Lentz, S. Trellenkamp, J.-m. Hartmann, J. Knoch, D. Buca, and Q.-t. Zhao, Vertical heterojunction Ge_{0.92}Sn_{0.08}/Ge gate-all-around nanowire pMOSFETs with NiGeSn contact, *Solid-State Electron.* **168**, 107716 (2020).
- [23] Y.-S. Huang, Y.-j. Tsou, C.-H. Huang, C.-H. Huang, H.-s. Lan, C. W. Liu, Y.-C. Huang, H. Chung, C.-P. Chang, S. S. Chu, and S. Kuppuraio, High-mobility CVD-grown Ge/strained Ge_{0.9}Sn_{0.1}/Ge quantum-well pMOSFETs on Si by optimizing Ge cap thickness, *IEEE Trans. Electron Devices* **64**, 2498 (2017).
- [24] W. Wang, D. Lei, Y.-C. Huang, K. H. Lee, W.-K. Loke, Y. Dong, S. Xu, C. S. Tan, H. Wang, S.-F. Yoon, X. Gong, and Y.-C. Yeo, High-performance GeSn photodetector and fin field-effect transistor (FinFET) on an advanced GeSn-on-insulator platform, *Opt. Express* **26**, 10305 (2018).

- [25] A. Vohra, C. Porret, D. Kohen, S. Folkersma, J. Bogdanowicz, M. Schaekers, J. Tolle, A. Hikavy, E. Capogreco, L. Witters, R. Langer, W. Vandervorst, and R. Loo, Low temperature epitaxial growth of Ge : B and Ge 0.99 Sn 0.01 : B source/drain for Ge pMOS devices: *in-situ* and conformal B-doping, selectivity towards oxide and nitride with no need for any post-epi activation treatment, *Jpn. J. Appl. Phys.* **58**, SBBA04 (2019).
- [26] C. E. Tsai, F. L. Lu, Y. C. Liu, H. Y. Ye, and C. W. Liu, Low contact resistivity to Ge using *in-situ* B and Sn incorporation by chemical vapor deposition, *IEEE Trans. Electron Devices* **67**, 5053 (2020).
- [27] M. Frauenrath, V. Kiyek, N. von den Driesch, M. Veillerot, E. Nolot, D. Buca, and J.-M. Hartmann, An in-depth study of the boron and phosphorous doping of GeSn, *ECS J. Solid State Sci. Technol.* **10**, 085006 (2021).
- [28] C.-E. Tsai, F.-L. Lu, P.-S. Chen, and C. Liu, Boron-doping induced Sn loss in GeSn alloys grown by chemical vapor deposition, *Thin Solid Films* **660**, 263 (2018).
- [29] J. Margetis, A. Mosleh, S. A. Ghetmiri, S. Al-Kabi, W. Dou, W. Du, N. Bhargava, S. Q. Yu, H. Profijt, D. Kohen, R. Loo, A. Vohra, and J. Tolle, Fundamentals of Ge_{1-x}Sn_x and Si_yGe_{1-x-y}Sn_x RPCVD epitaxy, *Mater. Sci. Semicond. Process.* **70**, 38 (2017).
- [30] Y. Shimura, S. Takeuchi, O. Nakatsuka, B. Vincent, F. Gencarelli, T. Clarysse, W. Vandervorst, M. Caymax, R. Loo, A. Jensen, D. Petersen, and S. Zaima, *In-situ* Ga doping of fully strained Ge_{1-x}Sn_x heteroepitaxial layers grown on Ge(001) substrates, *Thin Solid Films* **520**, 3206 (2012).
- [31] N. Taoka, G. Capellini, V. Schlykow, M. Montanari, P. Zaumseil, O. Nakatsuka, S. Zaima, and T. Schroeder, Electrical and optical properties improvement of GeSn layers formed at high temperature under well-controlled Sn migration, *Mater. Sci. Semicond. Process.* **57**, 48 (2017).
- [32] W. Wang, S. Vajandar, S. L. Lim, Y. Dong, V. R. D'Costa, T. Osipowicz, E. S. Tok, and Y. C. Yeo, *In-situ* gallium-doping for forming p+germanium-tin and application in germanium-tin p-i-n photodetector, *J. Appl. Phys.* **119**, 155704 (2016).
- [33] O. Nakatsuka, Y. Shimura, W. Takeuchi, N. Taoka, and S. Zaima, Development of epitaxial growth technology for Ge_{1-x}Sn_x alloy and study of its properties for Ge nanoelectronics, *Solid-State Electron.* **83**, 82 (2013).
- [34] N. Bhargava, J. P. Gupta, T. Adam, and J. Kolodzey, Structural properties of boron-doped germanium-Tin alloys grown by molecular beam epitaxy, *J. Electron. Mater.* **43**, 931 (2014).
- [35] M. Sathishkumar, T. Arun Samuel, and P. Vimala, A detailed review on heterojunction tunnel field effect transistors, in *2020 International Conference on Emerging Trends in Information Technology and Engineering (ic-ETITE)* (IEEE, New York, 2020), pp. 1–5.
- [36] B. Voigtländer, A. Zinner, T. Weber, and H. P. Bonzel, Modification of growth kinetics in surfactant-mediated epitaxy, *Phys. Rev. B* **51**, 7583 (1995).
- [37] C. R. Wang, B. H. Müller, E. Bugiel, T. Wietler, M. Bierkandt, K. R. Hofmann, and P. Zaumseil, Boron surfactant enhanced growth of thin Si films on CaF₂/Si, *J. Vac. Sci. Technol. A* **22**, 2246 (2004).
- [38] J. Klatt, D. Krüger, E. Bugiel, and H. J. Osten, Boron-controlled solid phase epitaxy of germanium on silicon: A new nonsegregating surfactant, *Appl. Phys. Lett.* **64**, 360 (1994).
- [39] U. W. Pohl, *Epitaxy of Semiconductors*, Graduate Texts in Physics (Springer International Publishing, Cham, 2020), pp. 469–520.
- [40] E. Simoen and C. Claeys, Diffusion and solubility of dopants in germanium, *Germanium-Based Technologies* (Elsevier, Amsterdam, 2007), pp. 67–96.
- [41] See Supplemental Material at <http://link.aps.org/supplemental/10.1103/PhysRevMaterials.7.074605> for additional details on growth and characterization of the samples presented in the manuscript, including XRD RSM, SEM, and AFM, top-view SEM image of a pure Ge film grown at 170 °C, SIMS data of Sn and In in samples A, B, E, I, Hall measurements of sample B, STEM of liquid segregation in sample F, TEM of defects in sample I, SEM EDX of SnIn droplets on sample F, and SEM of In liquid segregation in a pure Ge film.
- [42] C. Xu, C. L. Senaratne, R. J. Culbertson, J. Kouvetakis, and J. Menéndez, Deviations from Vegard's law in semiconductor thin films measured with X-ray diffraction and Rutherford backscattering: The Ge_{1-y}Sn_y and Ge_{1-x}Si_x cases, *J. Appl. Phys.* **122**, 125702 (2017).
- [43] J. Rathore, A. Nanwani, S. Mukherjee, S. Das, O. Moutanabbir, and S. Mahapatra, Composition uniformity and large degree of strain relaxation in MBE-grown thick GeSn epitaxial layers, containing 16% Sn, *J. Phys. D* **54**, 185105 (2021).
- [44] R. W. Olesinski and G. J. Abbaschian, The Ge-Sn (Germanium-Tin) system, *Bull. Alloy Phase Diagrams* **5**, 265 (1984).
- [45] K. A. Bratland, Y. L. Foo, T. Spila, H.-S. Seo, R. T. Haasch, P. Desjardins, and J. E. Greene, Sn-mediated Ge/Ge(001) growth by low-temperature molecular-beam epitaxy: Surface smoothing and enhanced epitaxial thickness, *J. Appl. Phys.* **97**, 044904 (2005).
- [46] P. Desjardins, T. Spila, O. Gürdal, N. Taylor, and J. E. Greene, Hybrid surface roughening modes during low-temperature heteroepitaxy: Growth of fully-strained metastable Ge(1-x)Sn(x) alloys on Ge(001)2X1, *Phys. Rev. B* **60**, 15993 (1999).
- [47] G. Xue, H. Z. Xiao, M. Hasan, J. E. Greene, and H. K. Birnbaum, Critical epitaxial thicknesses for low-temperature (20-100C) Ge(001)2x1 growth by molecular-beam epitaxy, *J. Appl. Phys.* **74**, 2512 (1993).
- [48] D. J. Eaglesham, Semiconductor molecular-beam epitaxy at low temperatures, *J. Appl. Phys.* **77**, 3597 (1995).
- [49] P. R. Pukite, A. Harwit, and S. S. Iyer, Molecular beam epitaxy of metastable, diamond structure Sn_xGe_{1-x} alloys, *Appl. Phys. Lett.* **54**, 2142 (1989).
- [50] A. Chroneos, Dopant-vacancy cluster formation in germanium, *J. Appl. Phys.* **107**, 076102 (2010).
- [51] R. Kube, H. Bracht, A. Chroneos, M. Posselt, and B. Schmidt, Intrinsic and extrinsic diffusion of indium in germanium, *J. Appl. Phys.* **106**, 063534 (2009).
- [52] T. B. Massalski, in *Binary Alloy Phase Diagrams*, 2nd ed., edited by T. B. Massalski, H. Okamoto, P. R. Subramanian, and L. Kacprzak (ASM International, Novelty, OH, 1990).
- [53] Here, we assume that the In incorporation rate is independent on the Sn flux, and thus the In surface concentrations of samples B and D are equal prior to segregation. Figure SM5 [41] confirms this is the case, by showing that the In concentrations below the surface of samples A and E are practically equal, despite their different Sn flux.

- [54] The present calculation of surface concentration of 1.2% at. In is clearly a simplification, but it is justified by looking at the composition of the segregation droplet in Fig. 2 (sample F), where the ratio of atomic densities n_{In}/n_{Sn} is equal to 7.6%. Additional SEM EDX measurements on different SnIn droplets in Fig. SM10 [41] confirmed the ratio n_{In}/n_{Sn} lies between 5% and 10% in sample F. Given the almost full miscibility of the SnIn liquid phase in this range of alloy composition [52], we can fairly assume that this ratio represents the ratio of surface adatom concentrations of the two elements on surface. In the case of sample F, with 5.9% at. Sn, this ratio thus yields a surface composition of $\sim (0.45 \pm 0.15)\%$ at. In, which is of the same order of magnitude of the 1.2% at. In obtained from SIMS measurements on sample B, grown under an equal In flux. This validates our initial argument on the enhancement of segregation due to the presence of In, especially considering that 0.45% at. $<$ 1.2% at. implies an even stronger influence of In on the segregation behavior of GeSn.
- [55] G. M. Pound, M. T. Simnad, and L. Yang, Heterogeneous nucleation of crystals from vapor, *J. Chem. Phys.* **22**, 1215 (1954).
- [56] J. A. Venables, G. D. T. Spiller, and M. Hanbucken, Nucleation and growth of thin films, *Rep. Prog. Phys.* **47**, 399 (1984).
- [57] M. A. Albao, J. W. Evans, and F.-C. Chuang, A kinetic Monte Carlo study on the role of defects and detachment in the formation and growth of In chains on Si(100), *J. Phys.: Condens. Matter* **21**, 405002 (2009).
- [58] A. E. Dolbak and B. Z. Olshanetsky, Diffusion of tin over clean silicon surfaces, *Phys. Solid State* **52**, 1293 (2010).
- [59] R. Dadashev, R. Kutuev, and R. Kutuev, Surface tension and density of indium-tin alloys, in *Proceedings of the International Symposium "Engineering and Earth Sciences: Applied and Fundamental Research" dedicated to the 85th anniversary of H.I. Ibragimov (ISEES 2019)* (Atlantis Press, Paris, France, 2019), Vol. 55, pp. 3024–3028.
- [60] *American Institute of Physics Handbook*, 3rd ed., edited by D. E. Gray (McGraw-Hill, New York, 1972).
- [61] For more information on the meaning of *activity coefficient*, the reader is directed to the brief, but complete review of Ref. [65].
- [62] V. Kumari and A. K. Mishra, Surface properties of liquid alloys, *High Temp. Materials Process.* **27**, 113 (2008).
- [63] R. Hultgren, P. D. Desai, D. T. Hawkins, and M. Gleiser, in *Selected Values of the Thermodynamic Properties of Binary Alloys*, edited by R. Hultgren (American Society for Metals, Metals Park, OH, 1973).
- [64] M. Nerding, L. Oberbeck, T. A. Wagner, R. B. Bergmann, and H. P. Strunk, Single to polycrystalline transition in silicon growth by ion-assisted deposition at low temperatures, *J. Appl. Phys.* **93**, 2570 (2003).
- [65] J. Tomiska, Thermodynamic activities of alloys, *Thermochim. Acta* **314**, 145 (1998).